Published in final edited form as:
Conf Proc IEEE Eng Med Biol Soc. 2013 July ; 2013: 5674–5677. doi:10.1109/EMBC.2013.6610838.

Improvement of Optical Coherence Tomography using Active Handheld Micromanipulator in Vitreoretinal Surgery

Sungwook Yang,
Robotics Institute, Carnegie Mellon University, Pittsburgh, PA 15213 USA

Marcin Balicki,
Department of Computer Science, Johns Hopkins University, Baltimore, MD 21218 USA

Trent S. Wells,
Department of Biomedical Engineering, Carnegie Mellon University, Pittsburgh, PA 15213 USA

Robert A. MacLachlan,
Robotics Institute, Carnegie Mellon University, Pittsburgh, PA 15213 USA

Xuan Liu,
Department of Electrical and Computer Engineering, Johns Hopkins University, Baltimore, MD 21218 USA

Jin U. Kang,
Department of Electrical and Computer Engineering, Johns Hopkins University, Baltimore, MD 21218 USA

James T. Handa,
Wilmer Eye Institute, Johns Hopkins University, Baltimore, MD 21287 USA

Russell H. Taylor, and
Department of Computer Science, Johns Hopkins University, Baltimore, MD 21218 USA

Cameron N. Riviere
Robotics Institute, Carnegie Mellon University, Pittsburgh, PA 15213 USA

Abstract

An active handheld micromanipulator has been developed to cancel hand tremor during microsurgery. The micromanipulator is also applicable in optical coherence tomography to improve the quality of scanning and minimize surgical risks during the scans. The manipulator can maneuver the tool tip with six degrees of freedom within a cylindrical workspace 4 mm in diameter and 4 mm high. The imaging system is equipped with a 25-gauge Fourier-domain common-path OCT probe. This paper introduces the handheld OCT imaging system and techniques involved and presents stabilized OCT images of A-mode and M-mode scans in air and live rabbit eyes. We show the first demonstration of OCT imaging using the active handheld micromanipulator *in vivo*.

I. Introduction

Optical coherence tomography (OCT) has emerged as an established technology in ophthalmology since its first demonstration in1991 [1] because it is capable of noninvasively imaging 3D structures with millimeter penetration, high resolution and speed

(camr@ri.cmu.edu).

[2]. In particular, endoscopic common path OCT offers several advantages such as a simple and compact configuration, a disposable and interchangeable tool usage, and cost-effectiveness. Moreover, it does not involve polarization and dispersion mismatch problems between reference and sample arms [3]. However, it is still challenging to acquire high quality OCT images during freehand operation due to hand tremor, which is defined as involuntary motion with maximum amplitude of about 100 μm at a frequency range from 7 to 17 Hz [4]. Hand tremor distorts tomography results by disturbing the probe location and orientation.

Since hand tremor occurs not only during freehand OCT imaging but also throughout the microsurgical procedure, robotic micromanipulators have been investigated as an aid to facilitate fine movement of surgical tools, compensating tremor [5-7]. As endoscopic OCT has recently progressed, robotic platforms have been adopted for OCT imaging, offering the aforementioned benefits [8-11]. Balicki *et al.* introduced single fiber OCT microsurgical instruments for robot-aided retinal surgery using the Johns Hopkins Eye Robot [8]. Given a surface profile from OCT data, the system enforces a safety barrier to prevent the surgical tip from touching a retinal surface. It can also maintain a certain distance from the surface and move the tool tip to a designated location after B-mode scanning. A handheld robotic-surgical tool, SMART, has recently been demonstrated to aid in micromanipulation by actively cancelling tremor cancellation using an OCT technique [10]. The OCT probe serves as a 1-D axial distance sensor, being incorporated with a single piezo-motor for active manipulation of the tool. However, it only provides one degrees of freedom (DOF) for both sensing and actuation along the longitudinal axis of the tool, whereas the tip fluctuates in 3-D due to hand tremor. Since the tremor in the transverse plane is not compensated, it may still cause distortion in OCT imaging.

The need for multi-DOF manipulation of tools has been addressed by development of a fully handheld instrument, known as “Micron,” [5, 12]. It senses its own motion and actively compensates involuntary and erroneous motion by manipulating the tool tip. The latest Micron prototype by Yang *et al.* is capable of maneuvering the tool tip with a range of motion of more than 4 mm with 6 DOF, while keeping the tool shaft stationary at the scleral incision point in intraocular surgery [13]. Utilizing this novel platform, we demonstrated the feasibility of automated intraocular acquisition of B-mode and C-mode OCT scans [11]. This paper describes how OCT imaging is stabilized by an active handheld micromanipulator and presents A-mode and freehand manual scan results in air and live rabbit eyes.

II. Methods

A. Active Handheld Micromanipulator

Micron is capable of maneuvering a tool tip in a cylindrical workspace of 4 mm in diameter and 4 mm high with 6 DOF. The manipulator is actuated by six ultrasonic linear motors (SQUIGGLE® SQL-RV-1.8, New Scale Technologies, Inc., USA) as shown in Fig. 1 (a). It also incorporates 6 LEDs to detect the motions of a tip and a handle, which are sensed by a custom-built microscale optical tracking system [14]. The maximum diameter of the instrument is 27. 5 mm and the overall length is 130 mm, excluding the length of the intraocular shaft which varies by the type of surgical tool.

In order to compensate hand tremor, Micron primarily uses a lowpass filter which attenuates the response beyond a corner frequency, 1.5 Hz. This is because voluntary motion is typically defined at below 2 Hz whereas hand tremor occurs at 7-14 Hz. Accordingly, the lowpass filter has unity gain at low frequency to preserve voluntary motion and high attenuation at 10 Hz and above to suppress high frequency tremor components. In addition

to this lowpass control mode, the manipulator is also capable of providing motion scaling. The motion scaling can be approximated by a shelving filter to provide a flat shelf near 1 Hz with gain of 1/3 [5]. Consequently, the manipulator operates in two control modes: *lowpass* to suppress hand tremor, and *scaling* to provide both tremor cancellation and scaling.

B. Fourier-domain Common-path OCT Integration

We adopted Fourier-domain common-path OCT (FD CP-OCT) that uses a common path interference configuration [15]. As the distal end of a single mode fiber is defined as a reference plane, a surface profile and a substructure can be extracted. The OCT system is primarily composed of a fiber-optic probe, a superluminescent diode (SLED), an optical coupler, and a custom-built spectrometer as illustrated in Fig. 2. The light source has a center wavelength of 840 nm with a spectral width of 50 nm. The spectral interference detected by the spectrometer is transferred to a workstation for signal processing. As a result, a single axial scan (A-scan) is acquired at a system sampling rate of 5 kHz with 10 bit digitized data, providing a theoretical axial resolution of 6.2 μm and practical imaging range of 2 mm in water.

The intraocular OCT probe consists of a standard single-mode fiber, with 9-μm core, 125-μm cladding, and an outer coating 245 μm in diameter, bonded within a 25-Ga. hypodermic needle [11]. For easy attachment of the OCT probe onto Micron, the probe is composed of multiple sheaths with hypodermic tubing of different diameters. The probe is fitted into the through hole of a Luer-Slip adaptor on Micron and coaxially aligned with the center of the manipulator. The probe length is designed to protrude 25 mm from the front cover of Micron to freely reach within the rabbit eye (about 15 mm in diameter). Once the OCT probe passes through a guide tube inside Micron and reaches the frontal part of Micron, it is affixed to the Luer adapter by a set screw.

All Micron data and status are sent to the workstation via an Ethernet using User Datagram Protocol (UDP) to minimize latency.

C. Testing

“A-scan” tests were first conducted during hold-still tasks for three cases: unaided (no cancellation), *lowpass*, and *scaling*. A surgeon was asked to maintain the tool tip at certain height from a fundus image printed on a paper for 12 s as shown in Fig. 3 (a). Each A-scan was accumulated as a single column in an OCT image over the 12 s duration as shown in Fig. 4.

In tests *in vivo*, under a board-approved protocol, a rabbit was anesthetized and the vitreous humor was removed from the eye by pars plana vitrectomy. In hold-still tasks, the surgeon followed the same protocols done in the previous freehand trials. In “M-scan” tests, the surgeon was required to scan a line across an area of interest in the eye while different control modes were enabled. Fig. 3(b) shows the retinal image and OCT profile during M-scan on the retinal surface of the rabbit eye.

III. Results

A. Open-Sky: A-mode Scan

Fig. 4 (a) represents A-scan images and short-time Fourier transform (STFT) of surface profiles depending on three types of control modes. The y axis depicts how the displacement between the distal end of OCT probe and the flat paper surface varies during hold-still trials of 12 s. This height variation is a combination of hand tremor and also voluntary motion to correct tip error from eye-hand feedback of the surgeon.

We found that the profiles were smoother in aided cases such as *lowpass* and *scaling* modes than in *unaided* cases as shown in Fig. 4 (a). This is because the tremor was canceled during aided trials such that the profile fluctuation was decreased. The standard deviations of the profiles were reduced by approximately 56 % in both aided trials compared with unaided cases. Significant differences between *lowpass* and *scaling* modes were not evident in the quantitative results summarized in Table I. Nevertheless, the profile acquired by *scaling* mode qualitatively appears much smoother than *lowpass* mode. In fact, scaling mode provides the surgeon finer control in voluntary motion and also scales excessive input by eye-hand feedback. In the spectrum analysis over the time, we definitely see noticeable difference between unaided and aided trials, specifically at the typical tremor band from 7 Hz to 15 Hz shown in STFT results of Fig. 4 (a).

B. In-vivo: A-mode Scan

Similar results were discovered during *in-vivo* trials, shown in Fig. 4 (b). Since the retina has a multilayer structure, for accurate evaluation of the performance, distance was measured from the brightest layer in the OCT images. The *lowpass* trial shows the most similarity to the open-sky trial in terms of reduction in both standard deviation and peak-to-peak deviation. In *scaling* mode, the reduction in the standard deviation is not as great as in the open-sky trial although the average spectral power density within the tremor frequency band is 4dB lower than in *lowpass* mode. The large standard deviation seems to be due to the gross motion of the tip by voluntary motion rather than instability from tremor. We also found that overall errors in trials *in vivo* were greater than the errors in the open-sky tasks. This seems to be a result of the awkward constraint at the sclera and the movement of the eye, which degrades the surgeon's manipulability. The data acquired through A-scan are summarized in Table 1 for hold-still tasks.

C. In-vivo: M-mode Scan

A manual scan (M-mode) under the scleral constraint is generally more challenging than hold-still tasks, since the movement of the tip creates reaction force from the sclera, and frequently moves the eye itself, rotating it in its socket.

M-scan results demonstrate that there is a qualitative difference among the scanned profiles in Fig. 5 and Fig. 6 (c). It is not possible to apply the same error metrics used in the hold-still task on the arbitrary profiles because each scan followed a different trajectory. However, we see there is an overall reduction in the tremor-caused variation of the profiles in Fig. 6 (c). The reduction of the average power is given by 13.1 and 11.4 dB in the frequency band of interest (7 to 20 Hz) as compared with the unaided case.

IV. Discussion

The data presented indicate that the quality of OCT imaging is improved by a handheld micromanipulator capable of cancelling hand tremor. We found noticeable attenuation on the variation of OCT profiles in both A-scans and M-scans, reflecting reduction of the hand tremor artifact. Compared to 1 DOF micromanipulators, Micron offers the advantage of suppressing both axial and transverse components of hand tremor and it does not rely on the OCT data for feedback.

This application is not limited to the compensation of hand tremor and the improvement of manual handheld OCT imaging. Feasibility of multidimensional scans of single fiber OCT has been shown by automatic manipulation using Micron in a previous study [11].

We have demonstrated the first handheld OCT imaging using Micron *in vivo*. Further experiments are required in order to obtain statistically significant results. Improvements in

Micron performance and in surgeons' familiarity with each control mode are expected to yield better performance in handheld OCT imaging. We will also be able to utilize a visual cue injection system [16] to guide the operator along predefined paths for M-scans, which would facilitate quantification of M-scan performance.

Acknowledgments

Research supported by the U.S. National Institutes of Health (grant nos. R01EB007969 and R01EB000526) and the Kwanjeong Educational Foundation.

References

[1]. Huang D, Swanson EA, Lin CP, Schuman JS, Stinson WG, Chang W, Hee MR, Flotte T, Gregory K, Puliafito CA, Fujimoto JG. Optical coherence tomography. Science. Nov.1991 254:1178–81. [PubMed: 1957169]

[2]. Kiernan DF, Mieler WF, Hariprasad SM. Spectral-domain optical coherence tomography: a comparison of modern high-resolution retinal imaging systems. Am. J. Ophthalmol. Jan.2010 149:18–31. [PubMed: 20103039]

[3]. Kang JU, Han JH, Liu X, Zhang K, Song CG, Gehlbach P. Endoscopic Functional Fourier Domain Common Path Optical Coherence Tomography for Microsurgery. IEEE J. Sel. Top. Quantum. Electron. Jul.2010 16:781–792. [PubMed: 22899880]

[4]. Singh SPN, Riviere CN. Physiological tremor amplitude during retinal microsurgery. Proc. IEEE 28th Ann. Northeast Bioeng. Conf. 2002:171–172.

[5]. MacLachlan RA, Becker BC, Tabarés JC, Podnar GW, Louis J, Lobes A, Riviere CN. Micron: an actively stabilized handheld tool for microsurgery. IEEE Trans. Robot. Feb.2012 28:195–212. [PubMed: 23028266]

[6]. Mitchell B, Koo J, Iordachita M, Kazanzides P, Kapoor A, Handa J, Hager G, Taylor R. Development and application of a new Steady-Hand manipulator for retinal surgery. Proc. IEEE Int. Conf. Robot. Autom. 2007:623–629.

[7]. Ueta T, Yamaguchi Y, Shirakawa Y, Nakano T, Ideta R, Noda Y, Morita A, Mochizuki R, Sugita N, Mitsuishi M, Tamaki Y. Robot-assisted vitreoretinal surgery: development of a prototype and feasibility studies in an animal model. Ophthalmology. Aug.2009 1161543:1538–43. e1–2. [PubMed: 19545902]

[8. Balicki M, Han JH, Iordachita I, Gehlbach P, Handa J, Taylor R, Kang J. Single fiber optical coherence tomography microsurgical instruments for computer and robot-assisted retinal surgery. Med. Image Comput. Comput. Assist. Interv. 2009; 12:108–15. [PubMed: 20425977]

[9]. Liu X, Balicki M, Taylor RH, Kang JU. Towards automatic calibration of Fourier-Domain OCT for robot-assisted vitreoretinal surgery. Opt. Express. Nov.2010 18:24331–43. [PubMed: 21164780]

[10]. Song C, Gehlbach PL, Kang JU. Active tremor cancellation by a "Smart" handheld vitreoretinal microsurgical tool using swept source optical coherence tomography. Opt. Express. 2012; 20:23414–21. [PubMed: 23188305]

[11]. Yang S, Balicki M, MacLachlan RA, Xuan L, Kang JU, Taylor RH, Riviere CN. Optical coherence tomography scanning with a handheld vitreoretinal micromanipulator. Proc.34th Annu. Int. Conf. IEEE Eng. Med. Biol. Soc. 2012:948–951.

[12]. Riviere CN, Ang WT, Khosla PK. Toward active tremor canceling in handheld microsurgical instruments. IEEE Trans. Robot. Autom. Oct.2003 19:793–800.

[13]. Yang S, MacLachlan RA, Riviere CN. Design and analysis of 6 DOF handheld micromanipulator. Proc. IEEE Int. Conf. Robot. Autom. 2012:1946–1951.

[14]. MacLachlan RA, Riviere CN. High-speed microscale optical tracking using digital frequency-domain multiplexing. IEEE Trans. Instrum. Meas. Jun.2009 58:1991–2001. [PubMed: 20428484]

[15. Liu X, Huang Y, Kang JU. Distortion-free freehand-scanning OCT implemented with real-time scanning speed variance correction. Opt. Express. Jul.2012 20:16567–16583.

[16]. Rodriguez Palma S, Becker BC, Lobes LA, Riviere CN. Comparative evaluation of monocular augmented-reality display for surgical microscopes. Proc. 34th Annu. Int. Conf. IEEE. Eng. Med. Biol. Soc.. 2012:1409–1412.

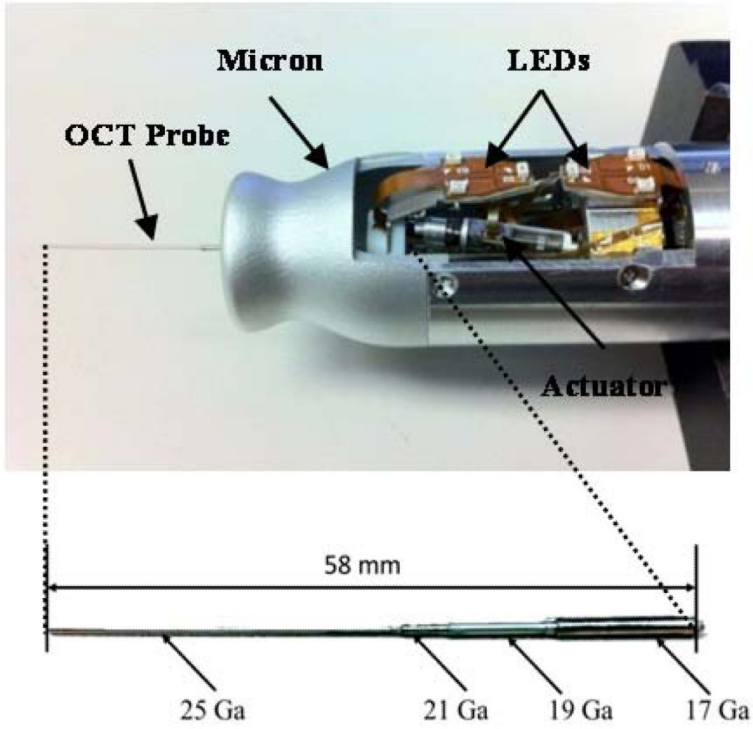

Figure 1.
Micron, an active handheld micromanipulator with an OCT probe (a) and the OCT probe with multiple sheaths of hypodermic tubing.

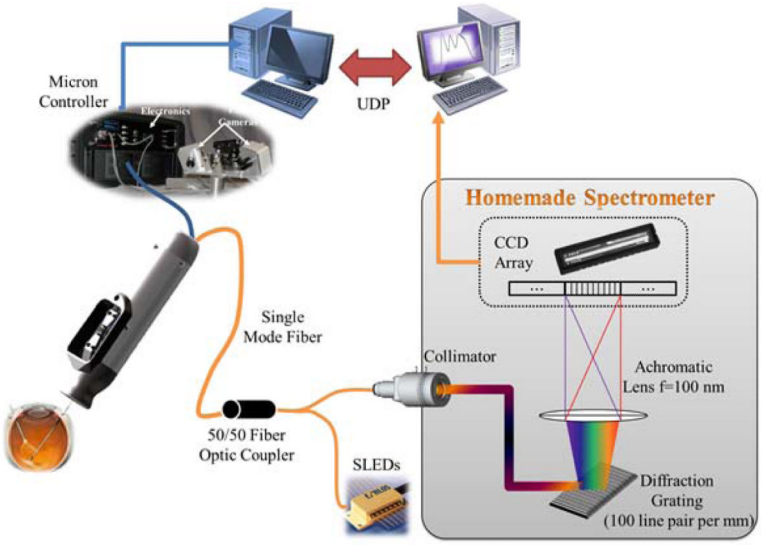

Figure 2.
Schematic diagram of a handheld OCT imaging system using Micron.

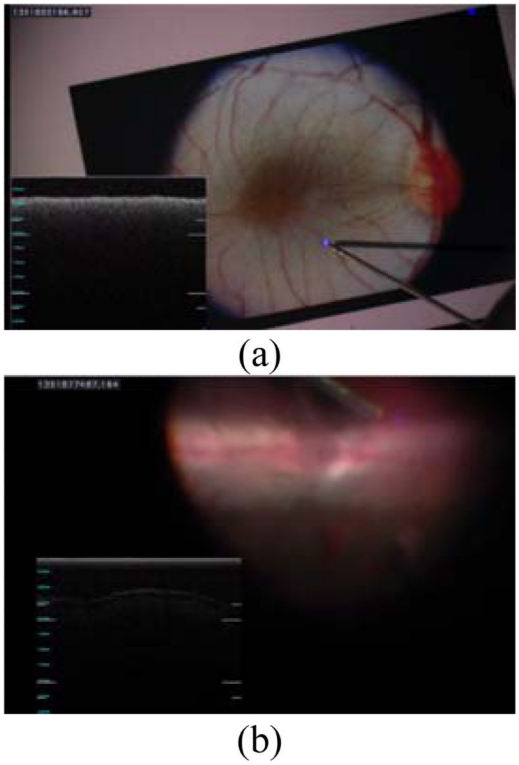

Figure 3.
(a) A-scans during hold-still task above a fundus image. (b) OCT scans (A-scan and M-scan) in a live rabbit eye.

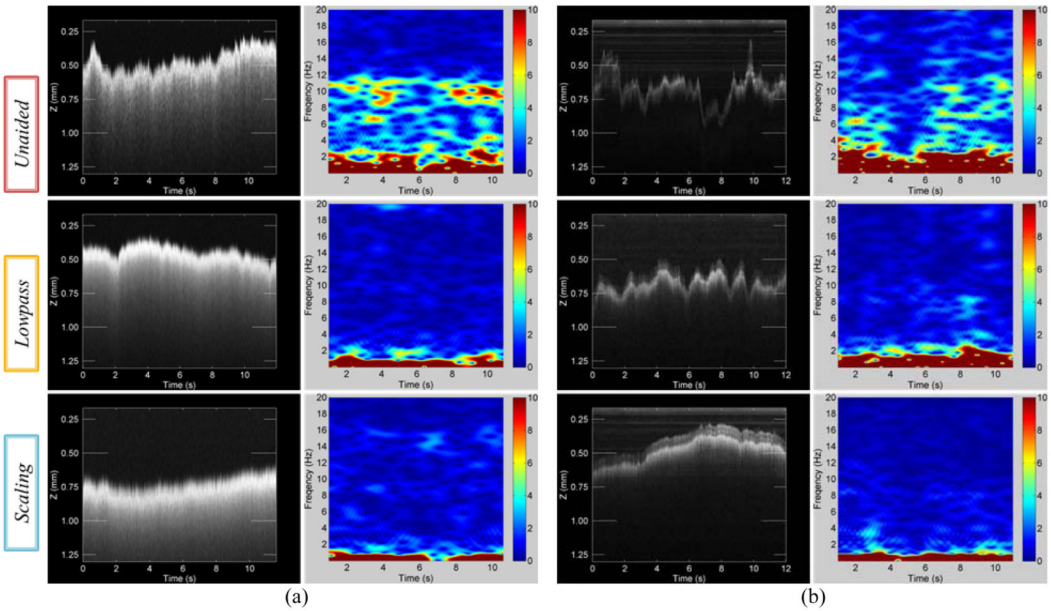

Figure 4.

Results of OCT scan images and short-time Fourier transform (STFT) of surface profiles for the control modes, arranged in descending order: *unaided, lowpass, and scaling*. (a) A-scans during hold-still task for 12 s in air. (b) A-scans during hold-still task in the live rabbit eye for 12 s.

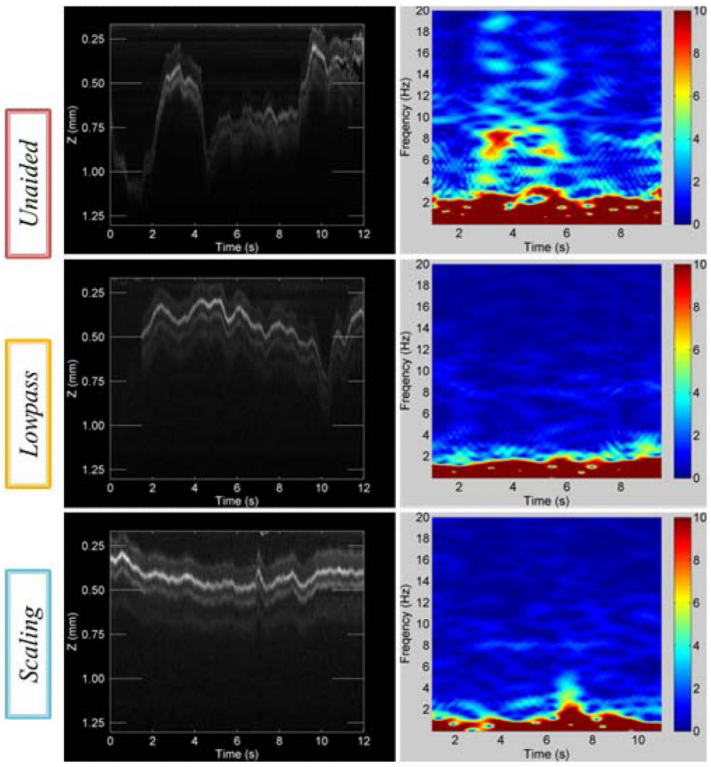

Figure 5.
Results of OCT M-scan images in the live rabbit eye and STFT of surface profiles.

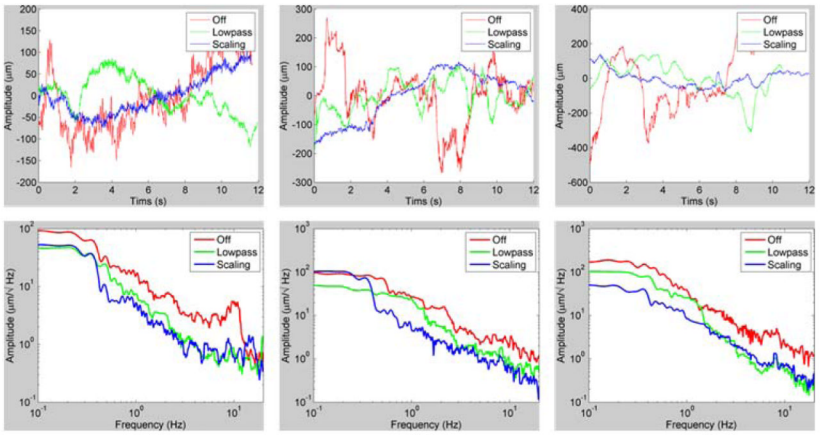

Figure 6.

Results of OCT scanned profiles (top) and power spectrogram (bottom). (a) A-scans during hold-still task in the air. (b) A-scans during hold-still task in the live rabbit eye. (c) M-scans, manually scanning a line of interest in the live rabbit eye. In the A-scans, the profiles are the axial deviation of the tip.

TABLE I

Errors during Hold-Still Tasks

Condition	Control	Std. (μm)	Pk-Pk (μm)	Power (μm^2/Hz)
Open-Sky (A-Scan)	Unaided	80 (100.0 %)	357 (100.0 %)	6.631 (0.0 dB)
	Lowpass	45 (55.9 %)	258 (76.9 %)	0.366 (−12.6 dB)
	Scaling	46 (56.9 %)	229 (70.0 %)	0.668 (−10.0 dB)
In-vivo (A-Scan)	Unaided	101 (100.0 %)	577 (100.0 %)	3.681 (0.0 dB)
	Lowpass	55 (55.0 %)	337 (74.9 %)	0.698 (−13.1 dB)
	Scaling	85 (84.4 %)	326 (68.7 %)	0.278 (−11.4 dB)

Std. = Standard deviation and Pk-Pk. =Peak-to-peak deviation.